*Acta of Bioengineering and Biomechanics*
*Vol. 25, No. 2, 2023*

Original paper
DOI: 10.37190/ABB-02262-2023-02

# The viscoelasticity, anisotropy and location-dependence of mechanical properties of rabbit iris investigated using uniaxial tensile tests

TAN LI[1, 2], XIAO QIN[3, 4], ZHICHENG LIU[3, 4], HAIXIA ZHANG[3, 4]*, LIN LI[3, 4]*

[1] Eye Institute of Shandong First Medical University,
Qingdao Eye Hospital of Shandong First Medical University, Qingdao, China.
[2] State Key Laboratory Cultivation Base, Shandong Provincial Key Laboratory of Ophthalmology, Qingdao, China.
[3] School of Biomedical Engineering, Capital Medical University, Beijing, China.
[4] Beijing Key Laboratory of Fundamental Research on Biomechanics in Clinical Application,
Capital Medical University, Beijing, China.

*Purpose*: Abnormal iris mechanical properties have been considered to be an important cause of pupillary-block and angle-closure glaucoma. In this research, viscoelasticity, anisotropy and location-dependence of mechanical properties of rabbit iris were investigated using uniaxial tensile test. *Methods*: Iris strips were taken along three directions: inner-circumferential direction (ICD), outer-circumferential direction (OCD) and radial direction (RD), respectively. Quasi-static tensile tests and stress–relaxation tests were applied on the iris strips. Then, the stress–stretch data was fitted with third order Ogden model; the stress–relaxation data was fitted with the third order Prony series model. Through comparing the tangent modulus and relaxation limit of the strips from different directions and locations, the viscoelasticity, anisotropy and location-dependence of mechanical properties of rabbit iris were explored. *Results*: The tangent moduli of iris at the stretch of 1.05 along ICD, OCD, and RD were 3.2 ± 1.4 kPa, 4.2 ± 2.6 kPa, 1.5 ± 0.8 kPa, respectively. Iris strips in ICD and OCD were found to have almost the same stress–relaxation behavior, and both relaxed slower than iris strips in RD. *Conclusions*: The mechanical properties of the iris were typically nonlinear, viscoelastic, anisotropic and location-dependent. The stress growth rate of the circumferential direction iris strip is significantly lower than that of RD and the stress–relaxation rate is significantly higher than that of the RD. That is, the iris is more prone to deformation in RD and the stress–retention ability after deformation in RD is weak, which is consistent with the fact that the iris bombe more likely happens in RD *in vivo*. The results of this study may also help us to establish a more accurate finite element model to simulate the flow field of humor aqueous and find the key factor of pupillary-block.

*Key words*: *iris, uniaxial tensile test, stress–relaxation, anisotropic mechanical property, location-dependence*

## 1. Introduction

Glaucoma is the first irreversible blinding disease in the world, with a prevalence of 3.54%. It is expected that the number of patients of glaucoma worldwide will reach 110 million by 2040, which is a major public health issue of global concerns [22]. Asians with shallow anterior chamber are more vulnerable to developing angle-closure glaucoma [1]. It is believed that pupillary block caused by abnormal iris morphology is the main risk factor for angle-closure glaucoma [17].

Iris morphology is determined by external and internal factors. The flow field of aqueous humor is the main external factor. The aqueous humor is secreted by the ciliary body, passes through the posterior chamber and iris-lens channel, enters into the anterior chamber. Because the iris-lens channel is narrow, aqueous humor has a high velocity and pressure here. This procedure creates a pressure difference between anterior and posterior chamber and causes iris bombe. The mechanical properties of iris are the main internal factor. Therefore, the mechanical property of the iris is of great importance to provide basic data to simulate the flow

* Corresponding authors: Haixia Zhang, Lin Li, School of Biomedical Engineering, Capital Medical University, Beijing 100069, China. E-mail: lil@ccmu.edu.cn, zhanghx@ccmu.edu.cn
Received: May 26th, 2023
Accepted for publication: September 18th, 2023

of aqueous humor in the anterior segment of eye and understand the mechanism of angle-closure glaucoma [6], [23].

There are many kinds of means to obtain the mechanical properties of iris, such as uniaxial tensile test, indentation experiments and the combination of finite element method with optimization algorithm. Zhang et al. [32] obtained the second order Ogden model parameters of rabbit iris *in vivo* by finite element method and optimization algorithm, which treated the iris as a kind of isotropic and homogeneous material. Barocas et al. performed uniaxial tensile test on the radial and azimuthal directions of bovine [5] and porcine iris [24], respectively, which paid attention to the mechanical anisotropy of the iris without the viscoelasticity. Barocas et al. [5] and Li et al. [13] also performed indentation experiments on the anterior and posterior surfaces of the porcine iris and rabbit iris, respectively, and revealed the mechanical asymmetry of the iris. Because of the little thickness of the iris, it was difficult to obtain the mechanical anisotropy of the iris by indentation experiment. Overall, a more comprehensive experimental design to characterize the mechanical properties of iris, including viscoelasticity, anisotropy and location-dependence, is necessary and urgent.

A great number of investigations have performed uniaxial tension tests on biological soft tissue to get its viscoelasticity, anisotropy and location-dependence of mechanical properties, primarily because of the ease of performance, convenience for small sized sample and accuracy of data from the tests [2], [3], [8].

Therefore, in this research, rabbit iris strips were taken along inner-circumferential direction (ICD), outer--circumferential direction (OCD) and radial direction (RD), respectively. Quasi-static tensile and stress–relaxation tests were performed on the iris strips. By comparing the results, the anisotropic and location-dependent mechanical properties of iris were revealed. These findings would help us to establish a more accurate finite element model to simulate the flow field of humor aqueous and find the key factor of pupillary-block.

# 2. Materials and methods

## 2.1. Experimental materials

All animal experiments were in accordance with the Declaration of Helsinki and relevant Chinese laws and regulations. Rabbits aged 6–7 months were provided by experimental animal department of Capital Medical University. Rabbits were euthanized by intravenous injection of 10 ml of 3% pentobarbital sodium. Both eyes were removed completely. Each eye was then cut open from the sclera, the vitreous and lens were removed and the iris was carefully detached intact. The iris was divided equally into three parts, the first part for quasi-static tensile test, the second part for stress–relaxation test and the third part for thickness measurement. The initial thickness of iris strip was recorded as $th_0$. For the parts of iris prepared for tensile test, each part was cut into strips by 1 mm wide double-bladed cutting tool in inner-circumferential direction (ICD), outer-circumferential direction (OCD) and radial direction (RD), respectively (Fig. 1A).

## 2.2. Experimental methods

The biomechanical tests were carried out using ElectroForce® 3100 mechanical testing system (Fig. 1B) at a room temperature of 22 ± 3 °C. High precision sensor with 0.5% force transducer's resolution and 250 g range was applied. Following section 2.1, while testing, iris strip was clamped on the stretch test ma-

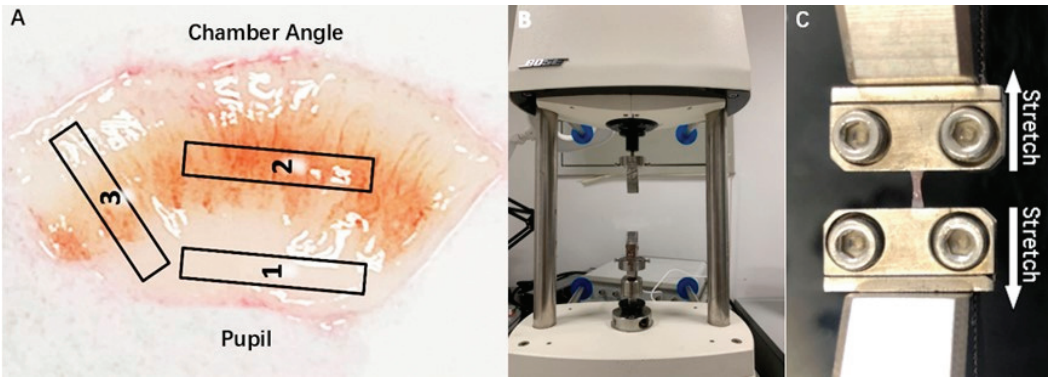


Fig. 1. Rabbit iris tissue and the definitions of inner-circumferential direction (ICD, marked with 1), outer-circumferential direction (OCD, marked with 2) and radial direction (RD, marked with 3)

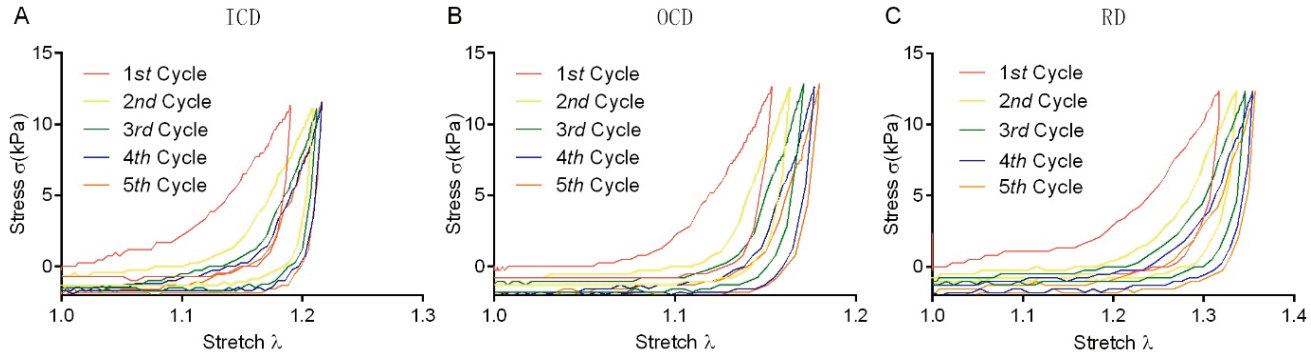


Fig. 2. Typical force–displacement curves of the iris strips during the preconditioning process in ICD (a), OCD (b) and RD (c).
The curves of the fourth and the fifth cycle basically overlapped, the preconditioning process had been completed

chine with a couple of custom-made clamps [30], [31] and the distance between the clamps was measured by a vernier caliper (Fig. 1C). This distance was regarded as the original length of the sample ($L_0$).

The preconditioning was performed at the loading rate of 0.02 g/s (force control, target was 0.4 g) and the unloading rate of –0.02 mm/s (distance control, target was the initial position), five cycles in total. The typical force–displacement curves of iris strips in ICD, OCD and RD during the preconditioning process are shown in Fig. 2. Then the tensile tests were conducted. The tensile speed was 0.02 mm/s in the quasi-static tensile test, while it was 0.4 mm/s in the stress–relaxation test. The elongation was 140% of $L_0$. In the stress–relaxation test, this stretched length was held for 300 s [30].

## 2.3. Mechanical data analysis

The stress $\sigma$ and the stretch ratio $\lambda$ are defined as $\sigma = \frac{F_t}{A_0}$, $\lambda = \frac{L}{L_0}$, where $F_t$ is the current applied force, $A_0$ is the original cross-sectional area, $L_0$ is the original length and $L$ is the current length. $A_0 = w_0 \times th_0$, $w_0$ and $th_0$ are original width and thickness of the iris strip, respectively. The normalized stress $G(t)$ is defined as $G(t) = \frac{F_t}{F_0}$, where $F_t$ is the current applied force, $F_0$ is the maximum applied force at the beginning of the relaxation.

Hyperelastic models have been used to describe the nonlinear elasticity of many kinds of soft materials. Ogden model is one of the most commonly used models [4], [7], [20], [30], [31]. For incompressible materials, the strain energy function of Ogden model is written as follows:

$$W = \Sigma_{i=1}^{N} \frac{2\mu_i}{\alpha_i^2}(\lambda_1^{\alpha_i} + \lambda_2^{\alpha_i} + \lambda_3^{\alpha_i} - 3), \quad (1)$$

where $\lambda_1$, $\lambda_2$ and $\lambda_3$ are the first, the second and the third stretch ratios, $\alpha_i$ and $\mu_i$ are material parameters, $N$ is the order. In this research, $\lambda_1 = \lambda$, $\lambda_2 = \lambda_3 = \lambda^{-\frac{1}{2}}$, stress $\sigma_1 = \sigma$, $\sigma_2 = \sigma_3 = 0$ [14], and the third order Ogden model ($N = 3$) is considered in this research. Then, we can get the following equation:

$$\sigma = \Sigma_{i=1}^{3} \frac{2\mu_i}{\alpha_i^2}(\lambda^{\alpha_i} - \lambda^{-\alpha_i/2}). \quad (2)$$

The stress–relaxation data was fitted by third order Prony series model [16], [18], [21] which is written as follows:

$$G(t) = 1 - \Sigma_{j=1}^{3} a_j(1 - e^{-t/\tau_j}), \quad (3)$$

where $a_j$ and $\tau_j$ are the viscoelastic material parameters of iris. Let $G(\infty)$ be $\lim_{t\to\infty} G(t)$, which gives the ultimate residual value of stress–relaxation, it is equal to $(1 - a_1 - a_2 - a_3)$. $\tau_1$, $\tau_2$ and $\tau_3$ are relaxation time constants.

For stress–stretch data, the material parameters can be estimated by optimizing (minimising) the stress-based nonlinear function: $M_{s1} = \Sigma_{i=1}^{N_1} [\sigma(t_i) - \sigma^i]^2$, where $t_i$ is the time points, $\sigma^i$ is the stress at a time point in loading process, $N_1$ denotes number of data points in extension and $\sigma(t_i)$ is the value calculated by Eq. (2).

Similarly, for stress–relaxation data, the material parameters can be estimated by optimizing (minimising) the stress-based nonlinear function: $M_{s2} = \Sigma_{j=1}^{N_2} [G(t_j) - s^j]^2$, where $t_j$ is the time points, $s^j$ is the normalized stress at a time point in relaxation process,

$N_2$ denotes number of data points in the stress–relaxation curves and $G(t_j)$ is the value calculated by Eq. (3).

All the computations were completed by applying the non-linear constrained global optimization in Mathematica™ packages (Wolfram Research, Inc., Champaign, IL, USA). Stochastic optimization method which was automatically assigned by the program package was used [11], [12]. The initial values of the unknown constitutive parameters were automatically assigned by the program package. The differential evolution method was applied.

## 2.4. Statistical analysis

One-Way ANOVA was applied to analyze the differences among iris samples in three directions under the same test conditions. $P < 0.05$ indicates a significant difference.

# 3. Results

## 3.1. Geometric parameters of the iris strips

A total of 14 eye balls from 7 rabbits were included in this study. The original length ($L_0$) and original thickness ($th_0$) of iris strips in the three directions under quasi-static tensile tests and stress–relaxation tests are listed in Table 1. The original width ($w_0$) of all iris strips was 1 mm.

Table 1. The original length ($L_0$) and original thickness ($th_0$) of iris strips (mean ± SD, $n = 14$)

| | Quasi-static tensile tests | | Stress–relaxation tests | |
|---|---|---|---|---|
| | $L_0$ [mm] | $th_0$ [μm] | $L_0$ [mm] | $th_0$ [μm] |
| ICD | 3.30 ± 0.27 | 291.5 ± 30.7 | 3.25 ± 0.31 | 305.2 ± 32.6 |
| OCD | 3.89 ± 0.45 | 305.8 ± 33.0 | 3.67 ± 0.35 | 318.1 ± 36.9 |
| RD | 3.48 ± 0.32 | 298.5 ± 32.1 | 3.54 ± 0.36 | 295.3 ± 33.8 |

## 3.2. Stress–stretch properties

The loss of strain energy in the 5th hysteresis loop, which is equal to the area enclosed by the loading and unloading curves, of iris strips in different directions and locations was shown in Fig. 3.

The stress–stretch curves shown in the Fig. 4 were significantly different in different directions and locations. All stress–stretch curves showed a typical "*J*-curve" feature. The tensile stress of the ICD under the same stretch was intermediate between those of OCD and RD. This result indicated that the iris strips in the RD were softer and more deformable.

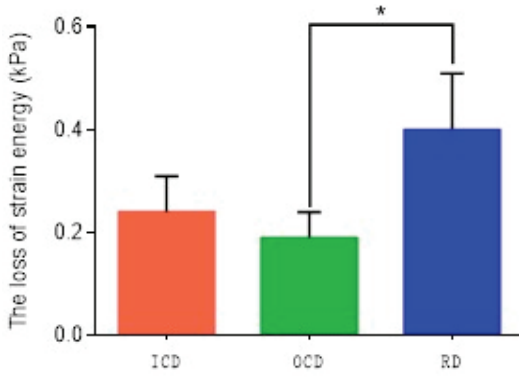


Fig. 3. The loss of strain energy in the 5th hysteresis loop of iris strips in different directions and locations (mean ± s.d.), $*p < 0.05$

Each stress–stretch curve was fitted by third order Ogden model ($R^2 > 0.95$). The parameters were shown in Table 2. The tangent modulus of iris under the stretch of 1.01, 1.03, 1.05, 1.10 and 1.15 were calculated (Fig. 5). Under the stretch of 1.03, the tangent modulus of iris in the ICD was obviously higher than that in the RD. Under the stretch of 1.05, 1.10 and 1.15, the tangent moduli of iris in ICD and OCD were obviously higher than that in the RD. Under the stretch of 1.10 and 1.15, the tangent moduli of iris in OCD were obviously higher than that in the ICD.

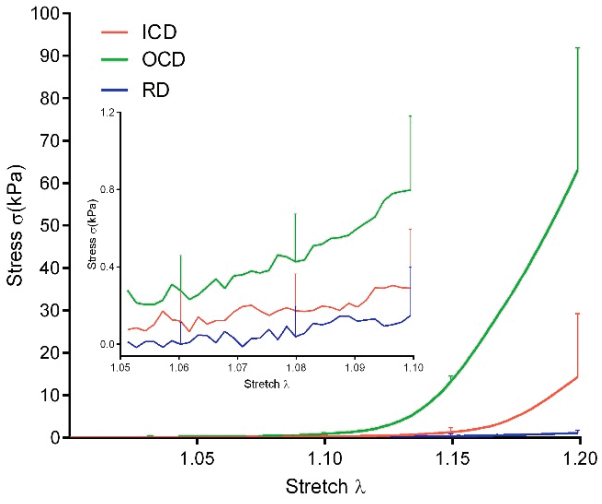


Fig. 4. Stress–stretch curves of iris stripes in the ICD, OCD and RD (mean ± SD). In order to show the changing trend of the curve more intuitively, only the standard deviations under the stretch of 1.05, 1.10, 1.15 and 1.20 are given in the larger figure (the standard deviations at 5% and 10% are small). The smaller figure is a magnified view of the stress–stretch curves in the 1.05–1.10 stretch range

Table 2. The parameters of third order Ogden model in different directions and locations ($n$ = 14)

| | | $\mu_1$ [kPa] | $\mu_2$ [kPa] | $\mu_3$ [kPa] | $\alpha_1$ | $\alpha_2$ | $\alpha_3$ | $R^2$ |
|---|---|---|---|---|---|---|---|---|
| ICD | mean | 0.02 | 0.17 | 0.52 | 51.60 | 14.51 | 4.26 | 0.99 |
| | SD | 0.01 | 0.08 | 0.28 | 23.26 | 5.95 | 1.36 | 0.01 |
| OCD | mean | 0.02 | 0.03 | 0.20 | 47.66 | 22.59 | 18.02 | 0.99 |
| | SD | 0.01 | 0.01 | 0.11 | 25.47 | 10.02 | 9.18 | 0.01 |
| RD | mean | 0.01 | 0.15 | 0.67 | 37.26 | 15.75 | 6.51 | 0.99 |
| | SD | 0.00 | 0.07 | 0.28 | 16.37 | 6.76 | 2.38 | 0.01 |

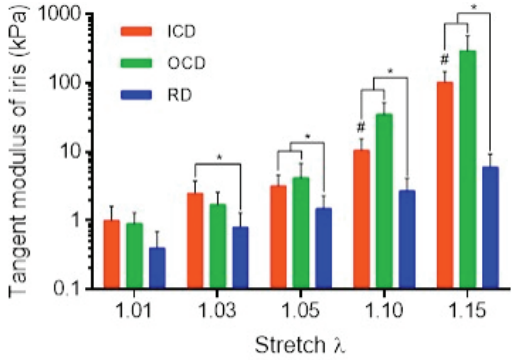


Fig. 5. The tangent modulus of iris (mean ± SD).
*$p$ < 0.05, compared to the tangent modulus of iris in RD;
#$p$ < 0.05, compared with the tangent modulus of iris in OCD

## 3.3. Stress–relaxation properties

The iris strips were stretched at a speed of 0.4 mm/s to achieve 140% of original length, and kept this length for 300 s. The normalized stress–relaxation curves of iris strips are shown in Fig. 6. When the iris strip was held to a constant, the significant stress–relaxation phenomena occurred. The velocity of stress–relaxation of ICD iris strips was almost the same as OCD iris strips, and obviously higher than that of the radial iris strips.

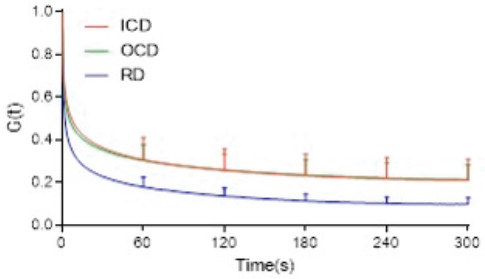


Fig. 6. The normalized stress–relaxation curves of iris strips in ICD, OCD and RD (mean ± SD).
The curves in ICD and OCD were almost coincident

Each stress–relaxation curve was fitted by the third order Prony series model ($R^2$ > 0.99). The fitted parame-

Table 3. The parameters of third order Prony series model in different directions and locations ($n$ = 14)

| | | $a_1$ | $a_2$ | $a_3$ | $\tau_1$ [s] | $\tau_2$ [s] | $\tau_3$ [s] | $R^2$ |
|---|---|---|---|---|---|---|---|---|
| ICD | mean | 0.20 | 0.21 | 0.38 | 94.21 | 11.48 | 1.12 | 0.99 |
| | SD | 0.04 | 0.03 | 0.07 | 28.51 | 4.31 | 0.69 | 0.00 |
| OCD | mean | 0.17 | 0.18 | 0.45 | 110.27 | 12.44 | 1.24 | 0.99 |
| | SD | 0.02 | 0.01 | 0.09 | 20.68 | 2.22 | 0.13 | 0.00 |
| RD | mean | 0.18 | 0.20 | 0.54 | 93.80 | 11.38 | 1.17 | 0.99 |
| | SD | 0.01 | 0.03 | 0.07 | 25.58 | 4.68 | 0.17 | 0.00 |

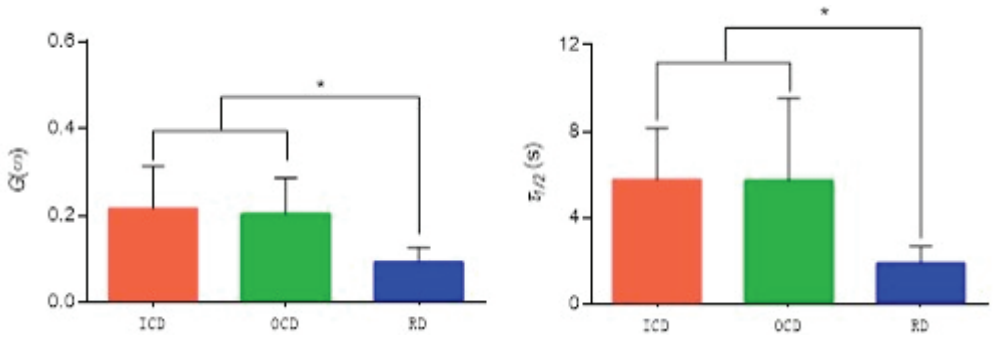


Fig. 7. The normalized relaxation limit (G(∞)) and the time for the initial stress of the iris strips to be relaxed to half its value during a stress–relaxation test ($\tau$_Υ(1⁄2)) (mean ± SD)

ters of stress–relaxation curves are shown in Table 3. The normalized relaxation limit of stress–relaxation ($G(\infty)$) which is equal to $(1 - a_1 - a_2 - a_3)$ and the time for the initial stress of the iris strips to be relaxed to half of the initial value during a stress–relaxation test ($\tau_{1/2}$) are shown in Fig. 7.

# 4. Discussion

In the present work, the uniaxial tensile experiments were performed on the rabbit iris along ICD, OCD and RD. At last, the anisotropy, viscoelasticity and location-dependence of mechanical properties of iris were revealed.

The materials parameters of iris in the Ogden model, including $\mu$ and $\alpha$, were obtained in this research, which were ranged from 0.01 to 0.67 kPa and 4.26 to 51.60, respectively. Parameter $\mu$ of the iris was obvious less than another study about the mechanical properties of the iris *in vivo* (from 37.7 to 43.05 kPa), which may be due to the difference between *in vivo* and *in vitro* experimental methods [32]. Simultaneously, parameter $\mu$ of the iris was obvious less than cornea (from 0.42 to 0.47 MPa) which illustrated that iris was more likely to deform than cornea [29]. Parameter $\alpha$ of the iris in this study was roughly equivalent to the iris and the cornea in the above two studies (from 48.07 to 54.26 and from 32.76 to 55.63, respectively).

There are three main components in iris, stroma, sphincter and dilator [13]. All of the iris strips in ICD, OCD and RD contain stroma, which is not the main reason for the difference of mechanical properties of different kinds of iris strips. However, sphincter is located in ICD and dilator is located in OCD, and the iris strip in RD contains both of these two muscles. Different components of muscles lead to the mechanical difference of iris strips in ICD, OCD and RD.

The stress–strain curves in the ICD and OCD were obviously different in the large strain (>10%) (Figs. 4 and 5), without difference in the viscoelasticity (Figs. 6 and 7). This indicates that the mechanical properties of iris are regionally dependent. At large strains, the ICD and OCD of iris strips show different mechanical properties. The regionally dependent viscoelastic properties of iris are not significant. Otherwise, the stress–strain curves in ICD/OCD were significantly higher than RD. Meanwhile, the stress–relaxation curves were obviously higher in ICD/OCD than RD. These results can explain the larger radial deformation of iris under physiological conditions.

In the quasi-static tensile test, the stress–stretch curves showed typically nonlinear and could be well fitted by the third order Ogden model ($R^2 > 0.95$). The tangent modulus (6.0 ± 3.2 kPa) of the iris strips in RD under the stretch of 1.15 in this study was approximately the same as the linear fitting results of the porcine radial iris strips (4.0 ± 0.9 kPa) in Barocas' research [24]. However, in the case of small stretch (1.01), the tangent modulus (0.4 ± 0.3 kPa) of the iris strips in RD in this study was significantly less than the result of Barocas' research [24]. The tangent modulus of the iris strips was obviously increased with the increase of strain. Therefore, the iris should be considered as a kind of nonlinear elastic material.

Indeed, the anisotropy and location-dependence of the iris had been paid attention in the previous research of Heys et al. [5]. They performed quasi-static tensile experiments on the iris strips and iris rings of bovine. Their ideas and testing results were similar to ours in several ways. First, they also preferred that tensile experiments of the radial iris strips mainly focus on the mechanical properties of dilator, the inner rings of iris mainly on the mechanical properties of sphincter and the outer rings of iris mainly on the mechanical properties of dilator. They used the neo-Hooken model to fit the force–displacement curves and obtained the elastic modulus of dilator and sphincter. Second, Heys' research also showed that the elastic modulus of the sphincter was greater than that of the dilator in the ICD/OCD, and both were much greater than that of the dilator in RD. Compared with the Heys' research, this research mainly has two improvements. First, in this research, the length–width ratio of the both radial and circumferential iris strips was greater than 3:1 (the initial width was 1 mm, and the initial length was greater than 3 mm), which is a necessary condition conducting uniaxial tensile tests. Second, since a sensor with high precision to measure the stress of iris under a small stretch was used in this research, the nonlinear stress–stretch relationship of rabbit iris strip was obtained, and the third order Ogden model was used in this research.

Stress–relaxation experiment is an important method to get the viscoelastic properties of materials, as well as one of the important means to study and verify the relationship between biological phenomena of biological tissues and mechanical microenvironment [15], [31]. Barocas [25] and Yoo [26] et al. have studied the stress–relaxation characteristics of iris based on the nano-indentation experiment, while the stress–relaxation experiment on the iris strips by uniaxial tensile experiment has rarely been reported before. Moreover, the data of this study illustrated that the stress–relaxa-

tion velocity of the iris strips in RD was significantly higher than that in ICD/OCD, as revealing the anisotropy on the viscoelasticity of the iris, which had never been reported before.

Since few studies have been conducted on iris stress––relaxation experiments using the stretching method, we consider the stress–relaxation experiments of other biological soft tissues when selecting the stretching amplitude used in the stress–relaxation experiment in this study. The existing human, pig and rabbit corneal relaxation experiments have a stretch of about 115–150% [27], [28]. The stretch of porcine amniotic membrane is about 140% [9]. The stretch of smooth muscle and connective tissue of the human trachea is about 150% [18]. With reference to the above research design, we set the tensile amplitude of 120%, 130% and 140% of the iris strip in the pre-experiment of the stress relaxation experiment. The results show that under the tensile amplitude of 140%, the iris strip will not be broken in all directions, and the stress––relaxation curves obtained are relatively smooth and stable. Therefore, 140% was adopted as the tensile amplitude for the stress–relaxation test in all directions of the iris strips.

Indentation is also a good method to get the location-dependence of the mechanical properties of iris. We have performed indentation on the iris root, mid-periphery and pupillary-margin of the rabbit iris in our previous research, finding that the iris in pupillary-margin was significantly stiffer than that in mid-periphery [13]. In order to investigate the location-dependence of the mechanical properties of iris under large deformation which is closer to the physiological state, we have also performed tensile test on the rabbit iris in this research. We found that stress–relaxation curves of the ICD and OCD iris strips almost coincided but the stress–stretch curves of OCD iris strips were obviously higher than that of ICD iris strips. This phenomenon illustrates that the hyperelasticity of ICD iris strips is stronger than that of OCD iris strips, but the viscoelasticity of these two iris strips is nearly the same.

As a biological soft tissue, the strain of the iris is about 20–40% *in vivo*, and it will be pulled off in rare cases. Therefore, in this study, we did not carry out the iris strip breaking experiment, nor did we consider the variability of maximum stress in tensile experiments according to the direction of loading.

In addition, the size of the eyeball and cornea increases with age and the curvature of the iris decreases [19]. Changes in these factors may cause changes in the aqueous humor flow field and intraocular pressure distribution, along with changes in the mechanical properties of the iris, including stress–strain properties, viscoelasticity, anisotropy and regional dependence et al. [13]. Studying the changes of iris mechanics with age is a very interesting topic, after all, the middle-aged and elderly people are the most prone to glaucoma [10].

There are also some limitations in this study. First, while this study has obtained the viscoelasticity, anisotropy and location-dependence of mechanical properties of iris tissue, it did not demonstrate the underlying causes, which are most likely related to the density and arrangement of the fiber. Second, the residual stress was not considered in our study, which should be incorporated to reflect the full mechanical state of the tissue. In order to reduce the complexity of considering residual stresses, we assumed a zero-stress state. Third, the iris tissue is mainly composed of stroma, dilator, sphincter, pigment epithelium, etc. Because the small size of each component, we could not isolate each component. In other words, the results of each direction (location) of iris strip were not the mechanical properties of pure components but the mean value of different components.

# 5. Conclusions

The mechanical properties of the iris were typically nonlinear, viscoelastic, anisotropic and location-dependent. The stress growth rate of the circumferential direction iris strip is significantly lower than that of the radial direction and the stress relaxation rate is significantly higher than that of the radial direction. That is, the iris is more prone to deformation in radial direction and the stress retention ability after deformation in radial direction is weak, which is consistent with the fact that the iris bombe more likely happens in radial direction *in vivo*. The results of this study may also help us to establish a more accurate finite element model to simulate the flow field of humor aqueous and find the key factor of pupillary-block.

## Conflict of interest

The authors declare that there are no conflicts of interest regarding the publication of this paper.

## Acknowledgement

This work was supported by National Natural Science Foundation of China (No. 31570952).

# References


[1] Aung T., Lim M.C., Chan Y.H., Rojanapongpun P., Chew P.T., *Configuration of the drainage angle, intraocular pressure, and optic disc cupping in subjects with chronic angle--closure glaucoma*, Ophthalmology, 2005, 112 (1), 28–32.

[2] Chen S., A NA, Roccabianca S., *A microstructurally inspired constitutive model for skin mechanics*, Biomech. Model Mechanobiol., 2020, 19 (1), 275–289.

[3] Christensen M.B., Oberg K., Wolchok J.C., *Tensile properties of the rectal and sigmoid colon: a comparative analysis of human and porcine tissue*, Springerplus, 2015, 4, 142.

[4] Fung Y.C., Fronek K., Patitucci P., *Pseudoelasticity of arteries and the choice of its mathematical expression*, Am. J. Physiol., 1979, 237 (5), H620–31.

[5] Heys J., Barocas V.H., *Mechanical characterization of the bovine iris*, J. Biomech., 1999, 32 (9), 999–1003.

[6] Heys J.J., Barocas V.H., Taravella M.J., *Modeling passive mechanical interaction between aqueous humor and iris*, J. Biomech. Eng., 2001, 123 (6), 540–547.

[7] Humphrey J.D., Strumpf R.K., Yin F.C., *A constitutive theory for biomembranes: application to epicardial mechanics*, J. Biomech. Eng., 1992, 114 (4), 461–466.

[8] Jia Z.G., Li W., Zhou Z.R., *Mechanical characterization of stomach tissue under uniaxial tensile action*, J. Biomech., 2015, 48 (4), 651–658.

[9] Kikuchi M., Feng Z., Kosawada T., Sato D., Nakamura T., Umezu M., *Stress relaxation and stress–strain characteristics of porcine amniotic membrane*, Biomed. Mater. Eng., 2016, 27 (6), 603–611.

[10] Lee S.S., Mackey D.A., *Glaucoma – risk factors and current challenges in the diagnosis of a leading cause of visual impairment*, Maturitas., 2022, 163, 15–22.

[11] Li L., Qian X., Wang H., Hua L., Zhang H., Liu Z., *Power type strain energy function model and prediction of the anisotropic mechanical properties of skin using uniaxial extension data*, Med. Biol. Eng. Comput., 2013, 51 (10), 1147–1156.

[12] Li L., Qian X., Yan S., Hua L., Zhang H., Liu Z., *Determination of the material parameters of four-fibre family model based on uniaxial extension data of arterial walls*, Comput. Methods Biomech. Biomed. Engin., 2014, 17 (7), 695–703.

[13] Li T., Qin X., Zhang H., Li L., Liu Z.. *Regional Changes of Iris Stiffness in the Rabbits Suffered from Chronic High Intraocular Pressure*, J. Med. Biol. Eng., 2021, 41 (2), 165–174.

[14] Ogden R.W., *Non-Linear Elastic Deformations*, Dover Publications, New York, 1997.

[15] Palko J.R., Pan X., Liu J., *Dynamic testing of regional viscoelastic behavior of canine sclera*, Exp. Eye Res., 2011, 93 (6), 825–832.

[16] Rassoli A., Fatouraee N., *Structural model for viscoelastic properties of pericardial bioprosthetic valves*, Artificial Organs, 2018, 42 (6), 630–639.

[17] Safa B.N., Wong C.A., Ha J., Ethier C.R., *Glaucoma and biomechanics*, Curr. Opin. Ophthalmol., 2022, 33 (2), 80–90.

[18] Safshekan F., Tafazzoli-Shadpour M., Abdouss M., Shadmehr M.B., *Viscoelastic Properties of Human Tracheal Tissues*, J. Biomech. Eng., 2017, 139 (1), 011007.

[19] Schuster A.K., Fischer J.E., Vossmerbaeumer U., *Curvature of iris profile in spectral domain optical coherence tomography and dependency to refraction, age and pupil size – the MIPH Eye&Health Study*, Acta Ophthalmol., 2017, 95 (2), 175–181.

[20] Stavropoulou E.A., Dafalias Y.F., Sokolis D.P., *Biomechanical and histological characteristics of passive esophagus: experimental investigation and comparative constitutive modeling*, J. Biomech., 2009, 42 (16), 2654–2663.

[21] Su P., Yang Y., Xiao J., Song Y., *Corneal hyper-viscoelastic model: derivations, experiments, and simulations*, Acta Bioeng. Biomech., 2015, 17 (2), 73–84.

[22] Tham Y.C., Li X., Wong T.Y., Quigley H.A., Aung T., Cheng C.Y., *Global prevalence of glaucoma and projections of glaucoma burden through 2040: a systematic review and meta--analysis*, Ophthalmology, 2014, 121 (11), 2081–2090.

[23] Wang W., Qian X., Song H., Zhang M., Liu Z., *Fluid and structure coupling analysis of the interaction between aqueous humor and iris*, Biomed. Eng. Online, 2016, 15 (Suppl. 2), 133.

[24] Whitcomb J.E., Barnett V.A., Olsen T.W., Barocas V.H., *Ex vivo porcine iris stiffening due to drug stimulation*, Exp. Eye Res., 2009, 89 (4), 456–461.

[25] Whitcomb J.E., Amini R., Simha N.K., Barocas V.H., *Anterior-posterior asymmetry in iris mechanics measured by indentation*, Exp. Eye Res., 2011, 93 (4), 475–481.

[26] Yoo L., Reed J., Shin A., Kung J., Gimzewski J.K., Poukens V., Goldberg R.A., Mancini R., Taban M., Moy R., Demer J.L., *Characterization of ocular tissues using microindentation and Hertzian viscoelastic models*, Invest. Ophthalmol. Vis. Sci., 2011, 52 (6), 3475–3482.

[27] Zeng Y., Yang J., Huang K., Lee Z., Lee X., *A comparison of biomechanical properties between human and porcine cornea*, J. Biomech., 2001, 34 (4), 533–537.

[28] Zhang D., Qin X., Zhang H., Li L., *Time-varying regularity of changes in biomechanical properties of the corneas after removal of anterior corneal tissue*, Biomed. Eng. Online, 2021, 20 (1), 113.

[29] Zhang D., Zhang H., Tian L., Zheng Y., Fu C., Zhai C., Li L., *Exploring the Biomechanical Properties of the Human Cornea In Vivo Based on Corvis ST*, Front Bioeng. Biotechnol., 2021, 9, 771763.

[30] Zhang H., Qian X., Li L., Liu Z., *Understanding the viscoelastic properties of rabbit cornea based on stress–relaxation tests and cyclic uniaxial tests*, J. Mech. Med. Biol., 2017, 17 (07), 1740035.

[31] Zhang H., Khan M.A., Zhang D., Qin X., Lin D., *Corneal biomechanical properties after FS-LASIK with residual bed thickness less than 50% of the original corneal thickness*, J. Ophthalmol., 2018, 2752945.

[32] Zhang K., Qian X., Mei X., Liu Z., *An inverse method to determine the mechanical properties of the iris in vivo*, Biomed. Eng. Online, 2014, 13, 66.